Structures of the Mo(V) Forms of Sulfite Oxidase from *Arabidopsis thaliana* by Pulsed EPR Spectroscopy†

Andrei V. Astashkin,⊥ Brian L. Hood,‡ Changjian Feng,⊥ Russ Hille,*,‡ Ralf R. Mendel,§ Arnold M. Raitsimring,⊥ and John H. Enemark*,⊥

Department of Chemistry, University of Arizona, 1306 East University Boulevard, Tucson, Arizona 85721-0041, Department of Molecular and Cellular Biochemistry, The Ohio State University, Columbus, Ohio 43210, and Institute of Plant Biology, Technical University Braunschweig, D-38106 Braunschweig, Germany

Received June 24, 2005; Revised Manuscript Received August 8, 2005

ABSTRACT: The Mo(V) center of plant sulfite oxidase from *Arabidopsis thaliana* (At-SO) has been studied by continuous wave and pulsed EPR methods. Three different Mo(V) EPR signals have been observed, depending on pH and the technique used to generate the Mo(V) oxidation state. At pH 6, reduction by sulfite followed by partial reoxidation with ferricyanide generates an EPR spectrum with *g*-values similar to the low-pH (*lpH*) form of vertebrate SOs, but *no* nearby exchangeable protons can be detected. On the other hand, reduction of At-SO with Ti(III) citrate at pH 6 generates a Mo(V) signal with large hyperfine splittings from a single exchangeable proton, as is typically observed for *lpH* SO from vertebrates. Reduction of At-SO with sulfite at high pH generates the well-known high-pH (*hpH*) signal common to all sulfite oxidizing enzymes. It is proposed that, depending on the conformation of Arg374, the active site of At-SO may be in "closed" or "open" forms that differ in the degree of accessibility of the Mo center to substrate and water molecules. It is suggested that at low pH the sulfite-reduced At-SO has coordinated sulfate and is in the "closed form". Reoxidation to Mo(V) by ferricyanide leaves bound sulfate trapped at the active site, and consequently, there are no ligands with exchangeable protons. Reduction with Ti(III) citrate injects an electron directly into the active site to generate the $[Mo^{V}{\equiv}O(OH)]^{2+}$ unit that is well-known from model chemistry and which has a single exchangeable proton with a large isotropic hyperfine interaction. At high pH, the active site is in the "open form", and water can readily exchange into the site to generate the *hpH* SO.

It has long been known that vertebrates possess a molybdenum enzyme, sulfite oxidase (SO),[1] that catalyzes the oxidation of sulfite to sulfate (*1*, *2*). Recently, similar molybdenum-containing enzymes that catalyze the oxidation of sulfite have been found in plants (*3*) and in certain bacteria (*4*). For SO from vertebrates, pulsed EPR spectroscopy has provided detailed insight into the structures of the Mo(V) species that are accessible on the catalytic pathway (*5*), as summarized below. Here, we extend our EPR studies to plant SO obtained from *Arabidopsis thaliana* (At-SO), whose crystal structure has recently been determined (*6*), and explore the similarities and differences in the Mo(V) centers of the plant and vertebrate enzymes.

The early findings that the Mo center in sulfite oxidase (SO) enzyme from vertebrates can be converted to a relatively stable Mo(V) paramagnetic state (*7*) gave rise to a substantial number of studies of SO employing continuous wave (CW)-EPR spectroscopy (*8*−*10*). As a result of these studies, three major forms of SO in the Mo(V) state producing distinctly different EPR spectra were observed and characterized (*10*): the so-called high-pH (*hpH*) form, generated at pH values of about 9 or higher; the low-pH (*lpH*) form, generated at pH values of about 7.5 or lower (depending on the concentration of Cl^- in the buffer); and the phosphate-inhibited (*Pi*) form that was observed at low pH in the presence of phosphate. In the EPR spectra of the *lpH* form, splittings due to an exchangeable ^{17}O (from ^{17}O-enriched H_2O) (*11*) and a single exchangeable proton (*10*) were observed, which indicated that the exchangeable ligand to Mo(V) in the *lpH* form was an OH group. The *hpH* and *Pi* forms, however, did not show any splittings attributable to ^{1}H or ^{31}P hyperfine interactions (*hfi*), respectively, and therefore, the nature of the exchangeable ligand in these forms was far from clear from the CW-EPR experiments (*10*). Later studies by high-resolution pulsed EPR techniques, including electron spin−echo envelope modulation (ESEEM) and electron−nuclear double resonance (ENDOR) spectroscopies, have contributed significantly to understanding of the structural details of the Mo(V)

† This work was supported by grants from the National Institutes of Health (GM-37773 to J.H.E. and ES-012658 to R.H.) and the National Science Foundation (DBI-0139459, DBI-9604939, and BIR-9224431) for construction of the pulsed EPR spectrometers.

* Corresponding authors. John H. Enemark: e-mail, jenemark@u.arizona.edu; phone, 520-626-8065; fax, 520-626-8065. Russ Hille: e-mail, hille.1@osu.edu; phone, 614-292-3545; fax, 614-292-4118.

⊥ University of Arizona.

‡ The Ohio State University.

§ Technical University Braunschweig.

[1] Abbreviations: SO, sulfite oxidase; At-SO, *Arabidopsis thaliana* sulfite oxidase; CW, continuous wave; *hpH*, high-pH form; *lpH*, low-pH form; *Pi*, phosphate-inhibited form; *hfi*, hyperfine interaction; *nqi*, nuclear quadrupole interaction; ESEEM, electron spin−echo envelope modulation; ENDOR, electron−nuclear double resonance.

10.1021/bi051220y CCC: $30.25
Published on Web 09/14/2005

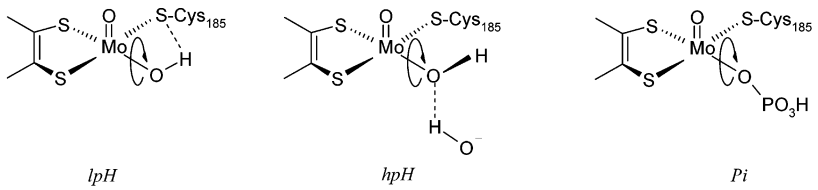

FIGURE 1: Structures of the Mo(V) center of chicken SO showing the nature of the exchangeable equatorial ligand for the *lpH*, *hpH*, and *Pi* forms as determined from high-resolution pulsed EPR spectroscopy (*5*). For each case, the equatorial ligand exhibits a distribution of torsional orientations along the Mo−O bond. The structure of the sulfate-coordinated form of *lpH* At-SO is proposed to be similar to the *Pi* form.

center in all three major forms of SO (Figure 1) (*12*−*16*). Recently, we have investigated human SO and showed that the structure of its Mo(V) center is identical to that of chicken SO (*13*, *17*).

Generally, the features of the EPR spectra of vertebrate SOs are independent of whether the Mo center is reduced by sulfite (a common practice), photochemically (*10*) or by titanium(III) citrate (*18*). However, when reduction of chicken SO was carried out in 4-morpholine-ethanesulfonic acid (Mes) buffer (pH 6.0), CW-EPR difference spectra gave evidence for a form of SO with principal *g*-values similar to those of *lpH* SO, but lacking the characteristic splittings from an exchangeable proton (*19*). This atypical form of SO was tentatively attributed to excess sulfite binding to the Mo(V) center, thereby blocking water access. No additional studies of this atypical form of SO have been described, and the mixture of signals present would make definitive high-resolution pulsed EPR studies very difficult.

For At-SO, unlike SO of vertebrates, we find that reduction of the Mo center by titanium(III) citrate at low pH in Bis-Tris propane buffer produces a Mo(V) EPR signal distinctly different from that generated by reduction by sulfite in the same buffer. The CW-EPR spectrum generated by Ti(III) citrate-reduced SO shows well-resolved proton splittings that are similar to those observed earlier for *lpH* chicken and human SOs (*10*, *13*), implying that Mo(V) is bound to a proton-containing ligand. However, the *lpH* EPR spectrum of At-SO generated by sulfite reduction and partial reoxidation with ferricyanide does not show any proton splittings and is similar to the atypical *lpH* spectrum observed earlier for chicken SO in Mes buffer (*19*). On the other hand, reduction of At-SO by sulfite at high pH produces CW-EPR results that are indistinguishable from those from chicken and human SO, consistent with the proposed $Mo^{V}{\equiv}O(OH_n)$ center (*14*). As we already learned from our previous studies of SOs, however, the lack of some features in CW-EPR spectra due to low spectral resolution does not necessarily prove that certain ligands are absent from the Mo(V) coordination sphere. Therefore, we have performed thorough high-resolution pulsed EPR studies of At-SO reduced by sulfite and Ti(III) citrate. These results are compared with data obtained for vertebrate SOs to lay the groundwork for understanding the intimate differences in the functioning of SOs from different organisms.

EXPERIMENTAL PROCEDURES

Recombinant wild-type *Arabidopsis thaliana* sulfite oxidase (At-SO) was expressed and purified as previously described (*3*). EPR spectra of the *lpH* and *hpH* forms of At-SO were obtained using samples in buffers containing 50 mM Bis-Tris propane (pH 6.0, *lpH*) and 100 mM CAPS (pH 10.0, *hpH*), respectively. Buffer exchange into D_2O was accomplished by concentrating the protein samples to 100 μL, then diluting to 3 mL with the appropriate buffer in D_2O. This procedure was repeated three times. The value of pD was calculated as $pD_{true} = pD_{apparent} + 0.4$ (*20*). For sulfite-reduced At-SO, the protein was reduced with a 30-fold excess of sodium sulfite and then reoxidized by about 1/2 equiv of ferricyanide (per enzyme) to maximize the Mo(V) signal. The samples were frozen in liquid nitrogen immediately after the addition of ferricyanide. For Ti(III) citrate-reduced *lpH* samples of At-SO in H_2O or D_2O, a stock solution of Ti(III) citrate was first prepared by a modified literature method (*18*), from 1 mL of $Ti(III)Cl_3$ (30% w/v in 2 M HCl) and 9 mL of well-degassed aqueous trisodium citrate solution (0.5 M) using a Schlenk line. The concentration of Ti(III) citrate was checked based on A_{340} ($\epsilon_{340} = 730\ M^{-1}\ cm^{-1}$) using a 100-fold diluted solution in 100 mM B-T propane buffer (pH 6.0). Approximately 1 mg of At-SO in 60 μL 50 mM Bis-Tris propane buffer (pH 6.0) was injected into an EPR tube, which was then transferred into a Schlenk tube. The Schlenk tube was pumped to obtain mild vacuum and then purged with Ar. This procedure was repeated three times to degas the protein. Next, 4 μL of 100-fold diluted Ti(III) citrate in well-degassed 100 mM Bis-Tris propane buffer (pH 6.0) was injected into the protein solution under Ar, and the reduced At-SO was frozen in liquid nitrogen immediately. The final ratio of [At-SO]/[Ti(III) citrate] was about 1:1.

The pulsed EPR experiments were performed on home-built, pulsed EPR spectrometers operating at microwave (mw) frequencies from 2 to 8 GHz (S and C bands) and from 8 to 18 GHz (X and K_u bands). The measurement temperature was about 20 K.

RESULTS

CW EPR Spectra of At-SO. Figure 2 shows the EPR spectra of *hpH* and *lpH* At-SO. The principal *g*-values for *hpH* SO (trace 1) of 1.989, 1.964, and 1.956 ($\pm$0.003) are identical to those reported originally (*3*) and similar to those in *hpH* chicken and human SOs.

The principal *g*-values corresponding to the main features of the EPR spectrum of sulfite-reduced *lpH* At-SO (trace 2), 2.005, 1.974, and 1.963 ($\pm$0.003), are also identical to those reported originally (*3*) and again similar to those in *lpH* chicken and human SOs. The unusual feature of the EPR spectrum of sulfite-reduced *lpH* At-SO is that it *does not show any splittings attributable to nearby exchangeable protons*, as is confirmed by the similarity of the spectra obtained for H_2O and D_2O solutions (traces 2 and 3 in Figure 2, respectively). The only feature that could potentially be interpreted as ^1H *hfi* splitting is the shoulder on the high-

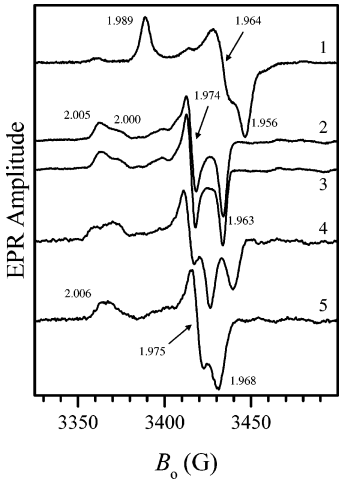

FIGURE 2: CW-EPR spectra of *hpH* At-SO (pH 10.0, trace 1), *lpH* At-SO reduced with sulfite (pH 6.0, traces 2 and 3), and with Ti(III) citrate (pH 6.0, traces 4 and 5). Traces 1, 2, and 4 are for the samples in H_2O, while traces 3 and 5 are for the samples in D_2O. Experimental conditions: mw frequency, 9.438 GHz (traces 1, 2, and 3) or 9.4496 GHz (traces 4 and 5); mw power, 200 μW; modulation amplitude, 1 G; modulation frequency, 100 kHz; measurement temperature, 77 K. In trace 4, the hyperfine splittings at g_Z, g_Y, and g_X are ~11, 10, and 13 G, respectively.

field side of the low-field EPR turning point (located at $g \sim 2.000$ (3375 G), trace 2 in Figure 2). This shoulder, however, does not disappear upon changing the buffer from H_2O to D_2O, which rules out its possible assignment to a proton *hfi*. In another study, addition of NaCl increased the intensity of the low-field feature with the shoulder, which was interpreted as evidence of proton splitting (Hood, B. L., Riebeseel, E., Schwarz, G., Mendel, R. R., Hemann, C. F., and Hille, R., to be submitted). However, at this point, the CW-EPR data are not sufficient to clearly define the origin of the shoulder on the low-field feature.

By contrast, if At-SO is directly reduced with titanium(III) citrate rather than sulfite, then the *lpH* spectrum shows the splittings attributable to a single nearby exchangeable proton (trace 4 in Figure 2). These splittings disappear in the spectrum of *lpH* At-SO in D_2O (trace 5 in Figure 2). The principal *g*-values found from spectrum 5 in Figure 2 are 2.006, 1.975, and 1.968 ($\pm$0.003), quite comparable with those of *lpH* chicken and human SOs.

To definitively establish the presence or absence of exchangeable proton(s) in sulfite-reduced At-SO, we have performed ESEEM and ENDOR measurements at various EPR positions (see below). Pulsed EPR was also used to study the *lpH* form of At-SO produced by reduction with titanium(III) citrate in order to accurately characterize the hyperfine (*hfi*) and quadrupole (*nqi*, in the case of D_2O) interaction tensors and compare them with those obtained for vertebrate SOs. For convenience of reference, we will denote below the largest, intermediate, and smallest principal *g*-values as g_Z, g_Y, and g_X, respectively.

Coordination Structure of the Mo(V) Center in hpH At-SO. The ESEEM and pulsed ENDOR spectra of *hpH* At-SO were essentially identical to those seen previously for *hpH* SOs from chicken and human (*13*−*15*, *17*), and therefore, we will not describe them in detail in this work. A simple demonstration of the presence of the neighboring exchangeable protons is provided by the ^{2}H ENDOR

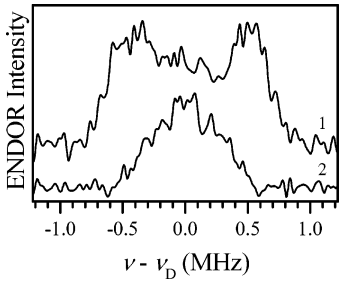

FIGURE 3: Trace 1, ^{2}H Mims ENDOR spectrum of *hpH* At-SO (pH 9.6) in D_2O recorded at $B_o = 5320$ G (near g_Y). Experimental conditions: mw frequency, 14.800 GHz; mw pulses, 3 × 10 ns; interval τ between the first and second mw pulses, 400 ns; interval *T* between the second an third mw pulses, 100 μs; RF pulse duration, 60 μs; temperature, ~20 K. Trace 2, ^{2}H Mims ENDOR spectrum of plant *lpH* (pH 6.0) SO in D_2O recorded at $B_o = 3410$ G (near g_Y). The mw frequency was 9.410 GHz. Other experimental conditions are the same as for trace 1.

spectrum of *hpH* At-SO shown in Figure 3, trace 1. This spectrum shows a hyperfine splitting between the major ^{2}H lines of about 1 MHz (~6.5 MHz as recalculated for a proton) typical for the protons/deuterons of the $OH_{(2)}$ ligand to the Mo(V) center in the *hpH* forms of chicken and human SO (*13*−*15*, *17*). From all the results obtained for *hpH* At-SO, we conclude that the overall geometry of the Mo(V) center in *hpH* At-SO is similar to that in chicken and human SO. The close similarity of the pulsed EPR spectra for *hpH* chicken SO and At-SO is also consistent with their very similar molybdenum coordination environments, as determined by X-ray crystallography (*6*, *21*).

Coordination Structure of the Mo(V) Center in Sulfite-Reduced lpH At-SO. The pulsed ENDOR spectra of weakly magnetically coupled protons in sulfite-reduced *lpH* At-SO in H_2O and D_2O buffers were similar to those obtained earlier for chicken and human *lpH* SOs (*13*), indicating the overall similarity of their active site structures. The significant difference in sulfite-reduced *lpH* At-SO compared to the chicken and human enzymes is the absence of a strongly magnetically coupled *exchangeable* proton in the Mo(V) center of At-SO. We therefore undertook an effort to detect possible more weakly coupled exchangeable protons in sulfite-reduced *lpH* At-SO using ESEEM and pulsed ENDOR. These methods have previously allowed unambiguous detection of the nearby exchangeable protons/deuterons in chicken and human SOs (*13*−*17*).

As an example, trace 2 in Figure 3 shows the ^{2}H ENDOR spectrum of *lpH* At-SO recorded at g_Y. This spectrum is considerably more narrow than that for *hpH* At-SO (trace 1 in the same figure), which immediately allows us to conclude that in the *lpH* At-SO the OH ligand is most likely missing from the Mo(V) coordination sphere. This conclusion is supported by the analysis of the ENDOR spectra in terms of the anisotropic *hfi* strength.

The width of the ^{2}H ENDOR spectra of *lpH* At-SO at any EPR position does not exceed 0.8 MHz, so the upper limit of the anisotropic *hfi* constant for the exchangeable deuterons can be estimated as $|T_\perp| \sim 0.4$ MHz. This estimate, however, does not include the effect of the nuclear quadrupole interaction (*nqi*) of deuterium nuclei. The quadrupole broadening of the ^{2}H ENDOR spectrum may be up to $(3/2)(e^2Qq/h)$, where e^2Qq/h is the quadrupole coupling constant. With

$e^2Qq/h \sim 0.25$ MHz for hydroxyl deuterons, we may evaluate a lower limit for the maximal anisotropic *hfi* constant of ^{2}H as $|T_\perp| \sim 0.2$ MHz. This latter estimate would, however, correspond to a maximal quadrupole broadening for the special situation of collinear *nqi* and *hfi* tensor axes. Therefore, the actual value of the maximal $|T_\perp|$ for deuterons should probably be somewhere between 0.2 and 0.4 MHz, and the average value of $|T_\perp| \sim 0.3$ MHz can be considered as a good estimate. This value corresponds to a minimum Mo···H distance of 3.3−3.4 Å, much larger than the 2.8 Å expected for protons of Mo−OH_2 or Mo−OH groups.

An independent estimate of the anisotropic *hfi* can be obtained from the time domain analysis of ^{2}H ESEEM damping (*22*). We have performed such an analysis for ^{2}H primary ESEEM in sulfite-reduced *lpH* At-SO (not shown) taking into account the anisotropic *hfi* and *nqi*. Assuming $e^2Qq/h \sim 0.25$ MHz, we found that the ESEEM amplitude and damping are mostly determined by approximately the two closest deuterons at a distance of about 3.4 Å. If $e^2Qq/h \sim 0.15$ MHz is assumed (which would correspond to an N−D or S−D group), the estimate is almost the same: about two deuterons at a distance of about 3.3 Å, consistent with the above estimation based upon the ENDOR analysis. Thus, all of our CW and pulsed EPR investigations indicate that the Mo(V) center of sulfite-reduced *lpH* At-SO does *not* have OH or OH_2 ligands, or any other ligands with nearby exchangeable protons.

Coordination Structure of the Mo(V) Center in Ti(III) Citrate-Reduced lpH At-SO. The Davies ENDOR spectra of weakly magnetically coupled protons in Ti(III) citrate-reduced *lpH* At-SO were very similar to the spectra of sulfite-reduced *lpH* At-SO and chicken SO, which show that the overall structures of the Mo(V) centers in these systems are similar. The nearby proton whose *hfi* was observed by EPR was also readily detected by ^{1}H and ^{2}H pulsed ENDOR, as well as by ESEEM.

Solid traces 1H−4H in Figure 4 show the ^{1}H Davies ENDOR spectra of Ti(III) citrate-reduced *lpH* At-SO in H_2O recorded at several points across the EPR spectrum. The high-frequency line of the nearby exchangeable proton in these spectra is located at $\nu - \nu_H \sim 15-25$ MHz, and its shape strongly depends on the observation position in the EPR spectrum. Similar data were obtained for *lpH* At-SO in a deuterated buffer (see solid traces 1D−4D in Figure 4 that represent ^{2}H refocused Mims ENDOR spectra rescaled to ^{1}H).

To determine the *hfi* parameters and the orientation of the *hfi* tensor relative to the *g*-frame, numerical simulations of ENDOR spectra were performed. To avoid complications due to the *nqi*, we concentrated our efforts on simulation of the ^{1}H ENDOR spectra only. As a result of these simulations, the following *hfi* parameters were found: the isotropic *hfi* constant, $a_{iso} = 35.5 \pm 0.5$ MHz; the anisotropic *hfi* constant (assuming an axial *hfi* tensor) $T_\perp = -5 \pm 0.5$ MHz; the polar ($\theta_h = 70° \pm 10°$) and azimuthal ($\varphi_h = 20° \pm 10°$) angles of the *hfi* axis orientation relative to the *g*-frame (assuming that the *g*-tensor axes *X*, *Y*, and *Z* correspond to the principal *g*-values 1.968, 1.975, and 2.006, respectively). To approximately reproduce the width of the ENDOR spectral lines, the isotropic *hfi* constant was Gaussian-distributed around the central value of 35.5 MHz with the distribution width between the maximal slope points of 4 MHz. The spectra simulated with such parameters are shown in Figure 4 by dashed lines.

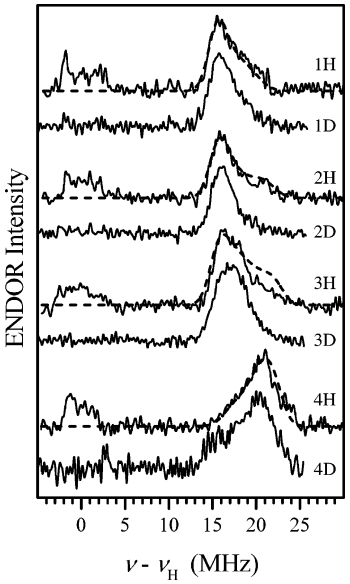

FIGURE 4: Solid traces 1H−4H, experimental ^{1}H Davies ENDOR spectra of Ti(III) citrate-reduced At-SO in H_2O recorded at B_o = 3370 G (near g_Z), 3389 G, 3408 G (near g_Y), and 3429 G (near g_X), respectively. Experimental conditions: mw frequency, 9.4315 GHz; mw pulses, 60 ns (180°), 30 ns (90°), and 60 ns (180°); time interval T between the first and second mw pulses, 20 μs; time interval τ between the second and third mw pulses, 400 ns; radio frequency pulse length, 5 μs. Solid traces 1D−4D, experimental ^{2}H refocused Mims ENDOR spectra of Ti(III) citrate-reduced At-SO in D_2O recorded at B_o = 6170 G (near g_Z), 6200 G, 6252 G (near g_Y), and 6270 G (near g_X), respectively, and rescaled to ^{1}H. Experimental conditions: mw frequency, 17.283 GHz; mw pulses, 3 × 20 ns (90°) and 15 ns (180°); time interval τ between the first and second mw pulses, 100 ns; time interval T between the second and third mw pulses, 55 μs; radio frequency pulse length, 20 μs. Dashed traces, simulated for a proton with the anisotropic *hfi* constant $T_\perp = -5$ MHz and the isotropic *hfi* constant a_{iso} being Gaussian-distributed around the central value of 35.5 MHz, with the width between the maximal slope points of 4 MHz. The orientation of the *hfi* tensor axis relative to the *g*-frame was described by the polar (θ_h) and azimuthal (φ_h) angles of 70° and 20°, respectively.

Including the nonaxiality of the *hfi* tensor in the simulation gave acceptable results if the largest anisotropic *hfi* component, T_{33}, was fixed at ∼10 MHz and the two smaller components were both within the limits $T_{11}, T_{22} \in [-4, -6]$ MHz (in that case, the orientation of the *hfi* tensor was described by Euler angles $\theta_h \approx 70°$, $\varphi_h \approx 20°$, and $\psi_h \approx 30°$). A larger difference between T_{11} and T_{22} (e.g., $T_{11} = -3$ and $T_{22} = -7$ MHz) resulted in poor agreement between the simulated and experimental spectra.

To establish the orientation of the *nqi* tensor axis for the nearby exchangeable deuteron, we have performed four-pulse ESEEM experiments with integration over the time interval τ between the first two mw pulses (*23*). In the integrated four-pulse ESEEM spectra, we were mostly interested in the sum combination line because this line exhibits the smallest *hfi* broadening and the largest *nqi* splittings, as compared to the fundamental lines or the difference combination line. To ensure a good orientational selectivity and to separate the sum combination line from fundamental lines, these experiments were performed at the K_u band frequency of 17.283 GHz. The spectra obtained in these experiments are shown in Figure 5.

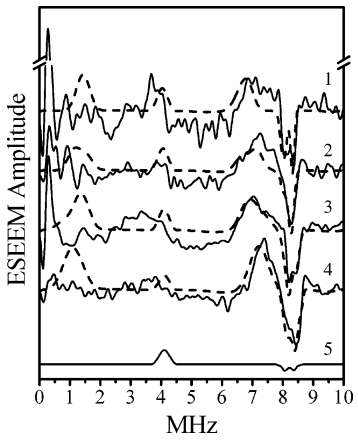

FIGURE 5: Solid traces 1, 2, 3, and 4, integrated (over τ) four-pulse ESEEM spectra of Ti(III) citrate-reduced *lpH* At-SO in D_2O recorded at $B_o = 6170$ G (near g_Z), 6200 G, 6252 G (near g_Y), and 6270 G (near g_X), respectively. Solid trace 5, matrix ESEEM calculated for $B_o = 6270$ G. In these spectra, the feature with negative amplitude located within the frequency range between 7.9 and 8.7 MHz is the sum combination line. Experimental conditions: mw frequency, 17.283 GHz; 90° mw pulses, 20 ns; 180° mw pulse, 15 ns. Dashed traces, simulated for a deuteron with the anisotropic *hfi* constant $T_\perp = -0.77$ MHz and the isotropic *hfi* constant a_{iso} being Gaussian-distributed around the central value of 5.45 MHz, with the width between the maximal slope points of 0.6 MHz (these values are obtained from the *hfi* parameters of the exchangeable proton, see Figure 4). The orientation of the *hfi* tensor axis relative to the *g*-frame was described by the polar (θ_h) and azimuthal (φ_h) angles of 70° and 20°, respectively. The *nqi* tensor was axial, with $e^2Qq/h = 0.25$ MHz, and the axis orientation relative to the *g*-frame described by the polar (θ_q) and azimuthal (φ_q) angles of 85° and 38°, respectively. The distant matrix deuterons with $e^2Qq/h = 0.25$ MHz were included in the simulations. They were assumed to be uniformly distributed around the Mo(V) center with the density of 0.018 $Å^{-3}$, starting from the minimal distance of 3.2 Å.

In the spectra of Figure 5, the sum combination line of the nearby exchangeable deuteron overlaps with that of the distant matrix deuterons, and the contribution of the latter to the total sum combination line has to be estimated independently. To make this estimate, we performed a numerical simulation of the matrix ^2H ESEEM observed in an X-band, two-pulse experiment. The X-band was used because it provides higher modulation amplitude for distant matrix deuterons. These simulations allowed the amplitude and width of the fundamental matrix line to be approximately reproduced if the distant deuterons were assumed to be uniformly distributed around the Mo(V) center with a density of 0.018 $Å^{-3}$, starting from the minimal distance of 3.2 Å. These parameters were used, therefore, in our simulations of the integrated four-pulse ESEEM to estimate the contribution of the distant matrix deuterons in the observed sum combination line.

As a result of our simulations, the polar (θ_q) and azimuthal (φ_q) angles of the *nqi* tensor axis relative to the *g*-frame were found to be about 85° ± 5° and 38° ± 5°, respectively. The integrated four-pulse ESEEM spectra simulated with these angles (while using the quadrupole coupling constant $e^2Qq/h = 0.25$ MHz for a hydroxyl deuteron and the *hfi* parameters determined above) are shown by dashed traces superimposed on the experimental solid traces in Figure 5. Using significantly smaller deuterium quadrupole coupling constants in the calculations ($e^2Qq/h < 0.2$ MHz) did not result in satisfactory fits to the experimental data. These findings imply that the observed deuteron belongs to an OD ligand.

Comparison of the simulated and experimental spectra in Figure 5 shows that there is a reasonable agreement between them in the high-frequency part of the spectra (which, importantly, is the region of the sum combination line that we are interested in) but that poor agreement is observed in the low-frequency part. This is due to the fact that the experimental ESEEM contains not only harmonics due to distant and neighboring protons and deuterons but also some additional low-frequency harmonics, the origin of which is not currently clear. Similar low-frequency ESEEM features were observed earlier for *lpH* chicken SO (*14*) and DMSO reductase (*24*). In the latter work, we made an assumption that they may originate from interaction of the unpaired electron of Mo(V) with chlorine nuclei present in the buffer (*24*).

DISCUSSION

Structural Implications of the Differences in Magnetic-Resonance Parameters of the Strongly Coupled Proton of lpH SO from Arabidopsis thaliana and Vertebrates. The *lpH* forms of Ti(III) citrate-reduced At-SO and vertebrate SO show similar splittings in their CW-EPR spectra; however, the isotropic *hfi* constant of the OH ligand proton in At-SO (35.5 MHz) is considerably greater than that in vertebrate SO (26−27 MHz) (*13, 17*) and is closer in magnitude to the *hfi* constant of the OH proton in DMSO reductase (about 31 MHz) (*24*). This large isotropic *hfi* constant is caused by the π-bonding interaction between the OH bond orbital and the d_{xy} orbital of Mo(V) where the unpaired electron is located. For simplicity, here and below, we neglect the implications of the structural distortions of the Mo complex in SO and still consider the Mo(V) orbital bearing the unpaired electron to be d_{xy}. The value of 35.5 MHz is close to the maximal values of isotropic *hfi* constants ever observed in model systems (~45 MHz) (*25, 26*), which indicates that the O−H bond lies near the d_{xy} orbital plane.

The angle θ_{hq} between the main axes of the *hfi* and *nqi* tensors of the exchangeable deuteron (for the sample in D_2O) is estimated to be about 23°, considerably smaller than ~51° expected in the case of the dipole interaction of the exchangeable deuteron with the unpaired electron on Mo(V). As discussed previously (*24*), such a small angle is caused by delocalization of the unpaired electron spin density onto the oxygen of the hydroxyl ligand. This spin density delocalization also leads to departure of the anisotropic *hfi* tensor from axial symmetry. For example, assuming the spin densities on Mo (ρ_{Mo}) and hydroxyl oxygen (ρ_O) of about 0.85 and 0.035, respectively (*27*), and assuming an sp^3 hybridization for the oxygen, one can estimate the total anisotropic *hfi* tensor to be [−6.2, −2.8, 9.0] MHz. The main axis of this tensor is in the Mo−O−H plane and is at an angle of about 43° to the Mo−O bond. The calculated angle θ_{hq} is about 28°, in qualitative agreement with $\theta_{hq} \approx 23°$ estimated from our experimental data. The largest calculated tensor component (9 MHz) approximately reproduces that observed experimentally (~10 MHz). On the other hand, the ratio between the two smaller components of the calculated tensor (~0.45) is somewhat smaller than the minimal value of ~0.67 estimated in our simulations. This difference may

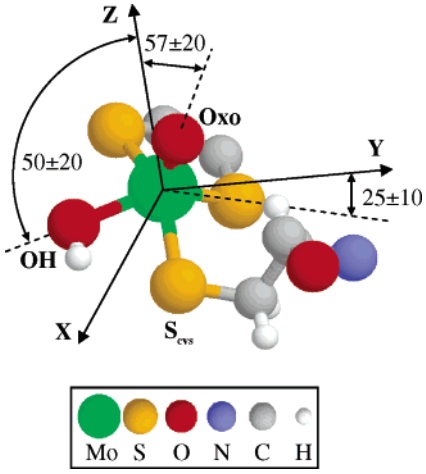

FIGURE 6: Orientation of the *g*-tensor and the exchangeable OH ligand with respect to the Mo(V) center of Ti(III) citrate-reduced *lpH* At-SO that was deduced from the *hfi* and *nqi* data for the exchangeable proton (deuteron) obtained in this work (see the text). The coordination geometry (without the hydroxyl proton) was taken from the X-ray crystallographic study of At-SO (PDB ID: 1OGP).

be attributed to a somewhat different actual spin density on oxygen in At-SO than was assumed in the calculation. An experiment in solution enriched in $H_2{}^{17}O$ should provide direct information on ρ_O. Interestingly, the anisotropic *hfi* tensor components found earlier for chicken and human *lpH* SOs (*13*, *17*) are on average about 50% greater than those in Ti(III) citrate-reduced *lpH* At-SO. This is probably due to different spin densities on the oxygen atom of the OH ligand for vertebrate and plant SOs.

Combining the *hfi* and *nqi* data obtained in this work for Ti(III) citrate-reduced *lpH* At-SO with the X-ray crystallographic data (*6*), we can propose the orientations of the *g*-frame and the ligand OH group with respect to the molybdenum coordination sphere. Assuming the OH bond to be parallel to the plane of the Mo(V) d_{xy} orbital, as discussed above, and the Mo(V) d_{xy} orbital plane to be perpendicular to the Mo≡O bond leads to the structure shown in Figure 6. Notably, axis *Y* of the *g*-tensor is oriented toward the α-proton of the cysteine ligand, in agreement with results of our ENDOR study of nonexchangeable protons in *lpH* SO (*14*). The angle between axis *Z* and the Mo≡O bond is large, although its lower limit is probably marginally acceptable. However, given the large number of assumptions involved in the derivation of the structure shown in Figure 6, it can only provide a qualitative guidance on the orientation of the *g*-frame and OH bond.

Biochemical Implications of the Differences in Reduction of At-SO by Ti(III) and Sulfite. The unusual feature of *lpH* At-SO is that the observed EPR signal depends on the reductant. Sulfite reduction of At-SO followed by partial reoxidation with ferricyanide yields a *lpH* EPR signal with *g*-values characteristic of the *lpH* SOs from vertebrates, but *no* nearby exchangeable protons are detected. On the other hand, direct one-electron reduction of At-SO by Ti(III) citrate efficiently generates the strong *lpH* Mo(V) EPR signal typical of vertebrate SO, with characteristic splitting from a nearby exchangeable proton with a large isotropic component and which can be assigned the structure of Figure 6. These two distinctly different types of *lpH* At-SO raise fundamental structural and mechanistic questions about the active sites of At-SO and vertebrate SO.

The crystal structures of At-SO and chicken SO show very similar overall structures of their molybdenum domains, with the active site lying at the bottom of a positively charged funnel (*6*). The entrance to this funnel is larger for chicken SO, but At-SO shows a more pronounced positive charge distribution that stretches almost across the entire width of the protein. The primary difference in the active site structures of At-SO and chicken SO is the conformation of Arg374 (Arg450 in chicken), and this residue is postulated to be crucial for substrate binding (*6*). In chicken SO, Arg450 is hydrogen-bonded to the sulfate anion that crystallizes in the substrate binding site to give a "closed form" of the active site. However, in the At-SO structure, there is no sulfate in the active site, and Arg374 is rotated away to give an "open form". It should also be kept in mind that the crystals of chicken SO were grown at pH 7.8 and those for At-SO at pH 9.2, whereas the *lpH* EPR experiments were done at pH ~6. Additionally, the molybdenum center of chicken SO is thought to have been reduced to Mo(IV) or Mo(V) in the crystal by exposure to the intense synchrotron X-ray source during data collection, whereas At-SO appears to be in the fully oxidized Mo(VI) state. Thus, the "closed form" of the active site is apparently favored for "reduced" SO in the presence of product sulfate, whereas the "open form" is favored for oxidized SO. It is interesting to note that the corresponding residue of an assimilatory nitrate reductase also appears to exist in comparable "open" and "closed" configurations (*30*), although this is a methionine (strictly conserved among the nitrate reductases) rather than the conserved arginine seen in the sulfite oxidases. Very recently, comparison of the structures of the resting and sulfate-bound forms of recombinant chicken SO showed, respectively, open and closed conformations for the side chain of Arg450 (*31*), which strongly supports our hypothesis for the behavior of the analogous residue (Arg374) in At-SO.

Next, we consider feasible reaction pathways for obtaining the Mo(V) forms of At-SO (Scheme 1) and vertebrate SO. For vertebrate SO, the generally accepted mechanism for generation of Mo(V) by sulfite reduction involves attack of sulfite upon the equatorial oxo-group of the dioxo−Mo(VI) center to generate an oxo−Mo(IV) center with coordinated sulfate. Hydrolysis of this enzyme−substrate complex gives product (sulfate), and one-electron oxidation of the Mo(IV) center by intramolecular electron transfer to the integral *b*-type heme of vertebrate SO generates the Mo(V) state. However, At-SO has no integral oxidant, and an external oxidant must be added after reduction with sulfite to generate the Mo(V) species. Thus, even though turnover of At-SO is very high *under catalytic conditions*, the process of generating EPR samples of At-SO could lead to novel Mo(V) structures.

Scheme 1 proposes a sequence of reactions and structures to account for our EPR results with At-SO. The central hypothesis is that at low pH the enzyme−product Mo(IV) complex of At-SO is trapped in the "closed form" and that the coordinated sulfate is not rapidly hydrolyzed, due in part to the narrower positively charged funnel of At-SO compared to chicken SO. This is consistent with the decreased catalytic activity of At-SO at low pH (Hemann, C. F., Hood, B. L., Fulton, M., Hänsch, R., Mendel, R. R., Kirk, M. L., and Hille,

Scheme 1: Proposed Reactions for Formation of the Mo(V) Forms of At-SO Observed by EPR

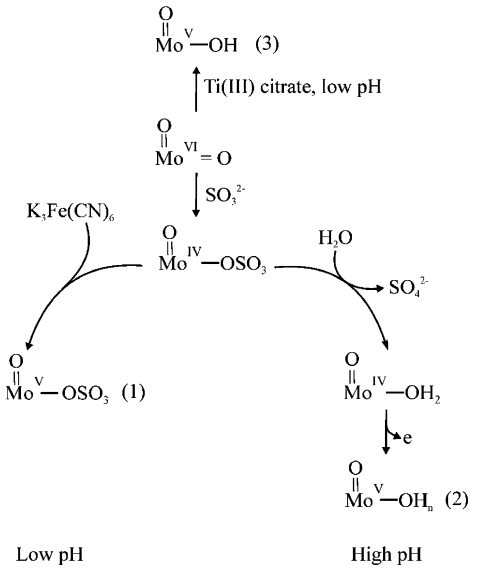

(1) is the At-SO species formed by sulfite reduction at low pH that shows no exchangeable protons; (2) is the *hpH* species that is formed in both At-SO and vertebrate SO; (3) is the *lpH* species formed in both At-SO and vertebrate SO by direct reduction of the Mo(VI) center.

R., submitted). Subsequent addition of 0.5 equiv of ferricyanide reoxidizes some of the Mo(IV) enzyme to Mo(V) but leaves it trapped in the "closed form" with bound sulfate and no nearby exchangeable protons (species 1 in Scheme 1). At high pH, the At-SO is in the "open form", bulk water can exchange readily into the site, and oxidation with ferricyanide generates the *hpH* EPR spectrum with nearby exchangeable protons that has been observed for all known sulfite oxidizing enzymes (species 2 in Scheme 1) (*13*−*15*, *17*, *28*).

Stoichiometeric one-electron reduction of oxidized enzyme (in the "open" configuration) with Ti(III) citrate provides an efficient direct pathway to the well-known *lpH* form with a large isotropic splitting (species 3 in Scheme 1). This process, which yields the Mo(V) state with both At-SO (present work) and chicken SO (*18*), is consistent with the known one-electron reduction chemistry of dioxo−Mo(VI) centers in model compounds, which generates strongly basic Mo(V) centers that are readily protonated to give $[Mo^{V}{\equiv}O(OH)]^{2+}$ units and which show a ^{1}H hyperfine splitting from an exchangeable proton of 30−45 MHz (*25*, *26*), similar to that of the *lpH* Mo(V) EPR signal from vertebrate sulfite oxidases and to that observed here for the *lpH* At-SO EPR signal generated by direct reduction with Ti(III) citrate.

Finally, we recognize that the implicit suggestion in Scheme 1 that two different equatorial ligands (sulfate and OH) give identical *g*-values for *lpH* At-SO is unprecedented for molybdenum enzymes. Model Mo(V) compounds have demonstrated that *g*-values are primarily determined by the number, nature, and spatial arrangement of the donor atoms (*29*). Small variations in *g*-values are typically observed for compounds with identical coordinated atoms but slightly different ligand skeletons; however, there are as yet no model Mo(V) compounds with sulfate ligands to provide benchmark EPR parameters for this postulated *lpH* form of At-SO.

CONCLUSIONS

We find that at low pH the Mo(V) EPR spectrum of At-SO depends on the nature of the reductant, sulfite versus Ti(III) citrate. Sulfite-reduced *lpH* At-SO is the first definitive example of a Mo(V) enzyme center with *no* detectable nearby exchangeable protons. These unusual EPR properties of At-SO are proposed to be directly related to the "open" and "closed" forms of the active site modulated by conformations of the active site arginine (Arg374) in combination with a more restricted substrate and water access to the active site of the plant enzyme than that found in vertebrate SOs. We hope that the present work will inspire new efforts to determine the crystal structures of SOs from various species under similar conditions and to conduct systematic mutagenesis studies of SO enzymes, especially of the conserved arginine associated with substrate binding. The hypothesized structural differences for *lpH* At-SO generated with different reductants also underscore the need for additional well-characterized model Mo(V) compounds that can be thoroughly investigated by pulsed EPR methods.

ACKNOWLEDGMENT

We thank Professor Caroline Kisker for helpful discussions and a preprint of ref *31* prior to publication.

REFERENCES

1. Hille, R. (1996) The mononuclear molybdenum enzymes, *Chem. Rev. 96*, 2757−2816.
2. Schindelin, H., Kisker, C., and Rajagopalan, K. V. (2001) Molybdopterin from molybdenum and tungsten enzymes, *Adv. Protein Chem. 58*, 47−94.
3. Eilers, T., Schwarz, G., Brinkmann, H., Witt, C., Richter, T., Nieder, J., Koch, B., Hille, R., Hansch, R., and Mendel, R. R. (2001) Identification and biochemical characterization of *Arabidopsis thaliana* sulfite oxidase—a new player in plant sulfur metabolism, *J. Biol. Chem. 276*, 46989−46994.
4. Kappler, U., Bennett, B., Rethmeier, J., Schwarz, G., Deutzmann, R., McEwan, A. G., and Dahl, C. (2000) Sulfite:cytochrome *c* oxidoreductase from *Thiobacillus novellus*—purification, characterization, and molecular biology of a heterodimeric member of the sulfite oxidase family, *J. Biol. Chem. 275*, 13202−13212.
5. Enemark, J. H., and Cosper, M. M. (2002) Molybdenum enzymes and sulfur metabolism, in *Metal Ions in Biological Systems; Molybdenum and Tungsten: Their Roles in Biological Processes* (Sigel, A., and Sigel, H., Eds.) Vol. 39, pp 621−654, Marcel Dekker, New York.
6. Schrader, N., Fischer, K., Theis, K., Mendel, R. R., Schwarz, G., and Kisker, C. (2003) The crystal structure of plant sulfite oxidase provides insights into sulfite oxidation in plants and animals, *Structure 11*, 1251−1263.
7. Cohen, H. J., Fridovich, I., and Rajagopalan, K. V. (1971) Hepatic sulfite oxidase—functional role for molybdenum, *J. Biol. Chem. 246*, 374−382.
8. Gutteridge, S., Lamy, M. T., and Bray, R. C. (1980) The nature of the phosphate inhibitor complex of sulphite oxidase from electron-paramagnetic-resonance studies using oxygen-17, *Biochem. J. 191*, 285−288.
9. Lamy, M. T., Gutteridge, S., and Bray, R. C. (1980) Electron-paramagnetic-resonance parameters of molybdenum(V) in sulphite oxidase from chicken liver, *Biochem. J. 185*, 397−403.
10. Bray, R. C., Gutteridge, S., Lamy, M. T., and Wilkinson, T. (1983) Equilibria amongst different molybdenum(V)-containing species from sulphite oxidase—evidence for a halide ligand of molybdenum in the low-pH species, *Biochem. J. 211*, 227−236.
11. Cramer, S. P., Johnson, J. L., Rajagopalan, K. V., and Sorrell, T. N. (1979) Observation of ^{17}O effects on Mo^{V} EPR spectra in sulfite oxidase, xanthine dehydrogenase, and $MoO(SC_6H_5)_4^-$, *Biochem. Biophys. Res. Commun. 91*, 434−439.

12. Astashkin, A. V., Feng, C. J., Raitsimring, A. M., and Enemark, J. H. (2005) ^{17}O ESEEM evidence for exchange of the axial oxo ligand in the molybdenum center of the high pH form of sulfite oxidase, *J. Am. Chem. Soc. 127*, 502−503.
13. Astashkin, A. V., Raitsimring, A. M., Feng, C. J., Johnson, J. L., Rajagopalan, K. V., and Enemark, J. H. (2002) Pulsed EPR studies of nonexchangeable protons near the Mo(V) center of sulfite oxidase: direct detection of the alpha-proton of the coordinated cysteinyl residue and structural implications for the active site, *J. Am. Chem. Soc. 124*, 6109−6118.
14. Astashkin, A. V., Mader, M. L., Pacheco, A., Enemark, J. H., and Raitsimring, A. M. (2000) Direct detection of the proton-containing group coordinated to Mo(V) in the high pH form of chicken liver sulfite oxidase by refocused primary ESEEM spectroscopy: structural and mechanistic implications, *J. Am. Chem. Soc. 122*, 5294−5302.
15. Raitsimring, A. M., Pacheco, A., and Enemark, J. H. (1998) ESEEM investigations of the high pH and low pH forms of chicken liver sulfite oxidase, *J. Am. Chem. Soc. 120*, 11263−11278.
16. Pacheco, A., Basu, P., Borbat, P., Raitsimring, A. M., and Enemark, J. H. (1996) Multifrequency ESEEM spectroscopy of sulfite oxidase in phosphate buffer: direct evidence for coordinated phosphate, *Inorg. Chem. 35*, 7001−7008.
17. Astashkin, A. V., Raitsimring, A. M., Feng, C., Johnson, J. L., Rajagopalan, K. V., and Enemark, J. H. (2002) The Mo−OH proton of the low-pH form of sulfite oxidase: comparison of the hyperfine interactions obtained from pulsed ENDOR, CW-EPR and ESEEM measurements, *Appl. Magn. Reson. 22*, 421−430.
18. Codd, R., Astashkin, A. V., Pacheco, A., Raitsimring, A. M., and Enemark, J. H. (2002) Pulsed ELDOR spectroscopy of the Mo(V)/Fe(III) state of sulfite oxidase prepared by one-electron reduction with Ti(III) citrate, *J. Biol. Inorg. Chem. 7*, 338−350.
19. Bray, R. C., Lamy, M. T., Gutteridge, S., and Wilkinson, T. (1982) Evidence from electron-paramagnetic-resonance spectroscopy for a complex of sulphite ions with the molybdenum center of sulphite oxidase, *Biochem. J. 201*, 241−243.
20. Glasoe, P. K., and Long, F. A. (1960) Use of glass electrodes to measure acidities in deuterium oxide, *J. Phys. Chem. 64*, 188−190.
21. Kisker, C., Schindelin, H., Pacheco, A., Wehbi, W. A., Garrett, R. M., Rajagopalan, K. V., Enemark, J. H., and Rees, D. C. (1997) Molecular basis of sulfite oxidase deficiency from the structure of sulfite oxidase, *Cell 91*, 973−983.
22. Dikanov, S. A., and Tsvetkov, Y. D. (1992) *Electron Spin Echo Envelope Modulation*, CRC Press, Boca Raton, FL.
23. Van Doorslaer, S., and Schweiger, A. (1997) A two-dimensional sum combination frequency pulse EPR experiment, *Chem. Phys. Lett. 281*, 297−305.
24. Raitsimring, A. M., Astashkin, A. V., Feng, C. J., Enemark, J. H., Nelson, K. J., and Rajagopalan, K. V. (2003) Pulsed EPR studies of the exchangeable proton at the molybdenum center of dimethyl sulfoxide reductase, *J. Biol. Inorg. Chem. 8*, 95−104.
25. Wilson, G. L., Greenwood, R. J., Pilbrow, J. R., Spence, J. T., and Wedd, A. G. (1991) Molybdenum(V) sites in xanthine oxidase and relevant analog complexes: comparison of Mo-95 and S-33 hyperfine coupling, *J. Am. Chem. Soc. 113*, 6803−6812.
26. Xiao, Z. G., Bruck, M. A., Doyle, C., Enemark, J. H., Grittini, C., Gable, R. W., Wedd, A. G., and Young, C. G. (1995) Dioxomolybdenum(VI) complexes of tripodal nitrogen-donor ligands: syntheses and spectroscopic, structural, and electrochemical studies, including the generation of EPR-active molybdenum(V) species in solution, *Inorg. Chem. 34*, 5950−5962.
27. Greenwood, R. J., Wilson, G. L., Pilbrow, J. R., and Wedd, A. G. (1993) Molybdenum(V) sites in xanthine oxidase and relevant analog complexes: comparison of oxygen-17 hyperfine coupling, *J. Am. Chem. Soc. 115*, 5385−5392.
28. Raitsimring, A. M., Feng, C. J., Kappler, U., Astashkin, A. V., and Enemark, J. H. (2005) Pulsed EPR studies of a bacterial sulfite-oxidizing enzyme with pH invariant hyperfine interactions from exchangeable protons, *Inorg. Chem.*, in press.
29. Cleland, W. E., Jr., Barnhart, K. M., Yamanouchi, K., Collison, D., Mabbs, F. E., Ortega, R. B., and Enemark, J. H. (1987) Syntheses, structures, and spectroscopic properties of 6-coordinate mononuclear oxo-molybdenum(V) complexes stabilized by the hydrotris(3,5-dimethyl-1-pyrazolyl)borate ligand, *Inorg. Chem. 26*, 1017−1025.
30. Fischer, K., Barbier, G. G., Hecht, H.-J., Mendel, R. R., Campbell, W. H., and Schwarz, G. (2005) Structural basis of eukaryotic nitrate reduction: crystal structures of the nitrate reductase active site, *Plant Cell 17*, 1167−1179.
31. Karakas, E., Wilson, H. L., Graf, T. N., Xiang, S., Jaramillo-Busquets, S., Rajagopalan, K. V., and Kisker, C. (2005) Structural insights into sulfite oxidase deficiency, *J. Biol. Chem.*, published online Jul 27.

BI051220Y